Supporting Information Section

Designer topological insulator with enhanced gap and suppressed bulk conduction in Bi_2Se_3/Sb_2Te_3 ultra-short period superlattices

Ido Levy[1,2], Cody Youmans[3,4], Thor Axtmann Garcia[1,2], Haiming Deng[3,4], Steven Alsheimer[3], Christophe Testelin[5], Lia Krusin-Elbaum[3,4], Pouyan Ghaemi[3,4], Maria C. Tamargo[1,2,4 *]

[1] Department of Chemistry, The City College of New York, New York, NY 10031
[2] Chemistry Program, Graduate Center of CUNY, New York, NY 10021
[3] Department of Physics, The City College of New York, New York, NY 10031
[4] Physics Program, Graduate Center of CUNY, New York, NY 10021
[5] Sorbonne Université, CNRS, Institut des NanoSciences de Paris, 4 Place Jussieu, F-75005 Paris, France
[*] Electronic address: mtamargo@ccny.cuny.edu

Abstract

The Supporting Information Section contains four sections:

A. Growth and Structural Characterization
B. Transport Measurements
C. Optical Measurements
D. Theoretical Modeling

A. Growth and Structural Characterization

A series of superlattice (SL) samples consisting of alternating thin layers of Bi_2Se_3 and Sb_2Te_3 were grown by molecular beam epitaxy. The samples were grown with different SL period thicknesses, as well as different ratios of individual Bi_2Se_3 to Sb_2Te_3 layer thickness. The SLs were always grown on a Bi_2Se_3 buffer layer that was deposited on the sapphire substrate first, to ensure a smooth surface for the Sb_2Te_3 material growth. All the samples consisted of seven periods of the two alternating materials. The initial Bi_2Se_3 buffer layer was grown using our previously reported procedure that ensures a very smooth and nearly twin free single layer crystal. [1]

The samples were characterized with high resolution X-ray diffraction (HRXRD) to establish their crystal quality. Scans of the (006) reflection of the zero-order SL peak, SL(0) allowed us to determine the effective composition of the samples (%Bi_2Se_3). To obtain the effective composition of each SL structure, we interpolated the 2θ value of the (006) SL(0) peak between the two end points of pure (006) Bi_2Se_3 (at 18.62°) and of pure Sb_2Te_3 (at 17.64°) according to equations 1 and 2.

(1) $$2\theta_{SL(0)} = X \times 2\theta_{Bi_2Se_3(006)} + (1 - X) \times 2\theta_{Sb_2Te_3(006)},$$

(2) $$\%Bi_2Se_3 = X \times 100 = \frac{SL(0) - Sb_2Te_3}{Bi_2Se_3 - Sb_2Te_3} \times 100$$

The full scan of the (006) SL(0) peak for each of the samples show multiple satellite peaks due to their SL structure, indicating that a layered structure with sharp interfaces and a well-defined periodicity was grown. The separation between the satellite peaks allowed us to calculate the thickness of the SL period. [2] Combining the value of the period thickness with the effective composition obtained from the SL(0) peak position, the individual thicknesses of the Bi_2Se_3 and Sb_2Te_3 layers can be calculated.

B. Transport Measurements

Transport measurements at 2K were made on several of the samples investigated. The carrier density of the five n-type samples studied are shown in Figure S1. A lower carrier density was obtained for the samples with the thinner SL periods. A very strong correlation between carrier concentration and the superlattice period was seen, consistent with the data shown in the main text. As with the data measured at 10K, shown in the main text, the value for the sample with the largest period of 14QL does not follow this trend, possibly due to the fact that at such a large period and the corresponding alternating layer thicknesses, the carriers are confined within the individual layers, and the material does not behave as a SL.

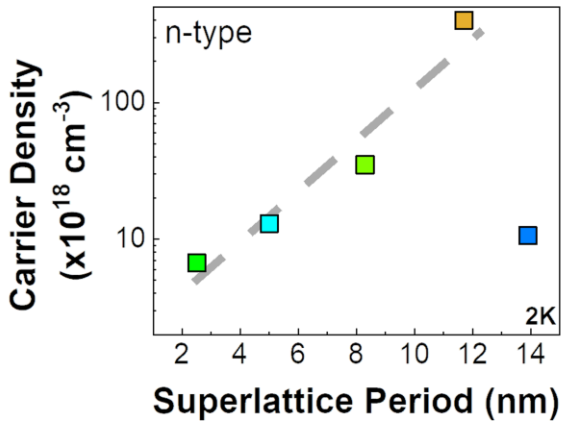

Figure S1: Carrier density obtained from Hall Effect measurements performed on several of the samples studied at 2K. The color of the squares corresponds to the effective composition, as indicated in the main text.

In systems such as the ones investigated here, that consist of alternating materials of two semiconductors, one typically n-type in the bulk, and the other typically p-type, and with type III or staggered band alignment, the question arises as to whether a two-carrier model would be needed to analyze the Hall effect data [3]. In a two-carrier system, the two types of carriers coexist in the material and contribute to the Hall effect. In that case, when the transverse Hall resistance (R_{xy}) is plotted over a sufficiently large magnetic field (B) range, a nonlinear behavior is seen as a function of B. Some evidence of two carrier effect in heterojunctions of Bi_2Te_3 and Sb_2Te_3 has been observed and reported by others [4]. To address this question, R_{xy} was measured for several of our samples at 2K as a function of magnetic field (B), with the magnetic field varying up to 3-4T, and in one case, for the thinnest period sample grown (period = ~2.5 nm), the value of B was varied up to 10T. The results are shown in Figures S2 (a and b). A highly linear behavior was consistently observed in all the samples. Thus, we conclude that in the short period SL structure, which is described by a new superlattice band structure, the system is well described by single carrier transport.

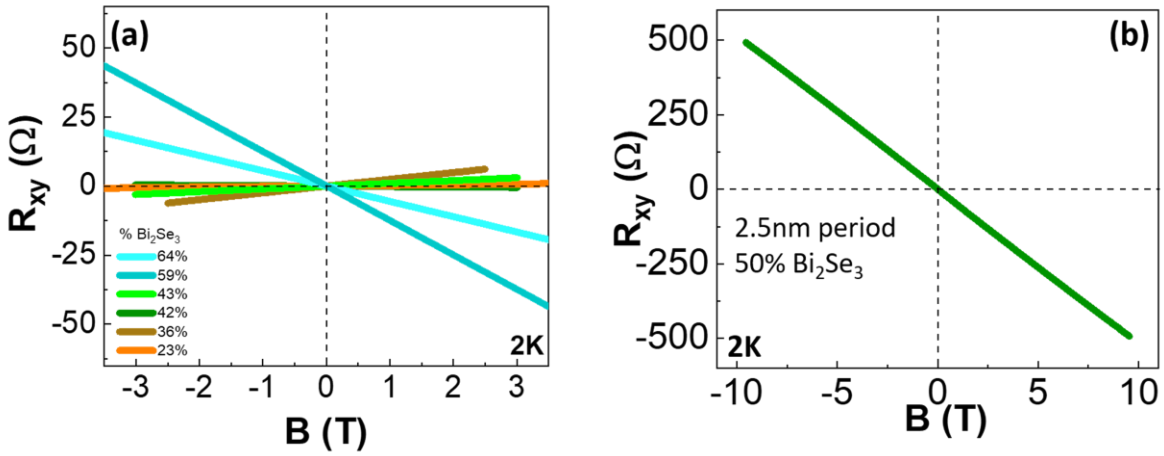

Figure S2: (a) Hall resistance of several of the samples grown, measured at 2K up to magnetic fields (B) of 3 to 4 Tesla. (b) Hall resistance for the thinnest period sample grown as a function of B, up to B values of 10T.

C. Optical Measurements

The optical properties have been explored by ellipsometric measurements performed at room temperature, with incident angles 60° and 70°, by using a commercial Woollam IR-VASE ellipsometer. Such approach has recently been used to study the Bi_2Se_3 gap energy, in epitaxial layers [5,6]. We have recorded the two ellipsometric angles, Δ and Ψ, defined by the ratio between the reflection coefficients of the p and s-polarized waves ($\frac{r_p}{r_s} = tan\Psi . e^{i\Delta}$). The optical constants have been determined from a layer plus substrate model, using the VASE software. Measurements and analysis have also been performed on a sapphire substrate for reference.

At room temperature, the gap energies E_{gap} are estimated at about 210-250 meV [7,8] and 115-140 meV [5,9], for Sb_2Te_3 and Bi_2Se_3, respectively. Moreover, the confinement effect is expected to be mainly observed for SL period shorter or equal to 5 QL. We have then focused on short period SL (5 and 8 QL periods) and on Sb_2Te_3, the bulk constituent material with the largest gap energy, for comparison.

Figure S3 shows the imaginary component ε_2 of the dielectric constant (related to absorption) versus photon energy. Those curves are very similar to what was observed on $Bi_2Se_{3-x}Te_x$ epitaxial layers[5]. For the Sb_2Te_3 layer and the 5QL period SL, an onset is clearly observed at an energy E_{opt}. This onset can be well determined by plotting the second derivative $\frac{d^2\varepsilon_2}{dE^2}$, from its inflection point. We have also performed measurements on an 8QL period SL and observed a different behavior, with no optical onset in the explored energy range (see fig. S3(b) for comparison with the 5QL period SL).

For the p-doped Sb_2Te_3 layer, the optical onset is at E_{opt} = 335 ± 10 meV. The optical transition is indirect, as already observed by IR absorption[7]. The gap energy can then by estimated from the equation $E_{gap} = E_{opt} - E_F$, with E_F the Fermi energy. From Hall resistivity, we have measured the hole concentration $p = 3.0 \times 10^{19} cm^{-3}$. The hole density-of-state effective mass m_h is known as increasing with the doping[10]. The doping being low, one can choose for m_h the lower observed mass, $m_h = 0.34\, m_0$[11]. One then estimates $E_F = 103\, meV$ and $E_{gap} = 232 \pm 10\, meV$, close to previous Sb_2Te_3 gap measurements[7].

We have then followed the same procedure for the 5QL period SL, with a doping $n = 1.1 \times 10^{19} cm^{-3}$. From the dielectric component ε_2 and its second derivative (see main text), we can estimate $E_{opt} = 403 \pm 10\ meV$. According to our calculations, one expects an indirect transition and the relation $E_{gap} = E_{opt} - E_F$. Nonetheless, a lower bound of the gap energy can be obtained by assuming a direct transition and the relation $E_{gap} = E_{opt} - \left(1 + \frac{m_e}{m_h}\right) E_F$.

The SL gap energy will be minimized by choosing the smallest effective mass values (higher Fermi energy). Further studies have to be done on the SL band parameters, but one can assume that the effective carrier masses are in between the Sb_2Te_3 and Bi_2Se_3 masses. For Bi_2Se_3 and Sb_2Te_3, respectively, the hole effective masses are $m_h = 0.24\, m_0$[12] and $0.34\, m_0$[11], and the electron effective masses are $m_e = 0.14\, m_0$[12] and $0.45\, m_0$ [13]. Taking Bi_2Se_3 masses, one then gets $E_F = 129\, meV$, and $E_{gap} = 200 \pm 10\ meV$. An indirect transition would lead to $E_{gap} = 274 \pm 10\ meV$. By comparing these values with the measured Sb_2Te_3 gap ($232 \pm 10\, meV$), one obtains a SGE in the range 102 ± 16 %, very close to the predicted value of 105 % (see fig. 3(b), main text). A similar observation has been done on another 5QL-period SL. As said previously, we have observed no optical onset for the 8QL period SL [see fig. S3(b)]. Since the doping and the Fermi energy of the 8QL SL are higher than in the 5QL SL, this indicates a low gap energy, in agreement with a SGE < 30 %, and E_{gap} < 70 meV.

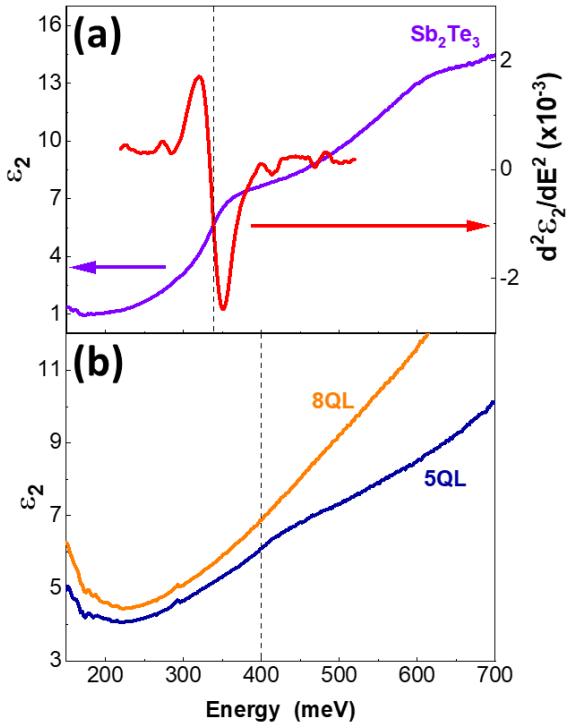

Figure S3: Ellipsometry measurements: (a) Imaginary component of the dielectric constant ε_2 (purple trace) and second derivative $\frac{d\varepsilon_2}{dE^2}$ (red trace), at room temperature, for a 60 nm Sb_2Te_3 layer; a dashed line indicates the optical transition onset E_{opt}. (b) Imaginary component of the dielectric constant ε_2, also a room temperature, for two SL samples with a period of 5QL (2 Sb_2Te_3 QL- 3 Bi_2Se_3 QL) (blue trace) or 8 QL period (4 Sb_2Te_3 QL- 4 Bi_2Se_3 QL) (orange trace). A dashed line indicates the optical transition onset E_{opt} for the 5QL sample as described in the main text, Figure 3(d). No evidence of an optical transition is seen in the 8QL sample.

Finally, we have performed transmission measurement at room and liquid nitrogen (LN) temperature. A 5QL-SL has been mounted on a cold finger in a cryostat. The transmission (and the derived absorption) has been measured with a ThermoScientific Nicolet 6700 Fourier Transform Infrared (FTIR) spectrometer and a LN-cooled MCTA detector. Fig. S4 shows the absorption measured at 300 and 77K for the sample (5QL-SL on a sapphire substrate); a clear peak, barely visible at RT, appears at 77K, at an energy very close to the one measured in ellipsometry. For comparison, absorption has been measured on a single sapphire substrate at RT. These preliminary measurements agree very well with the optical transition seen in ellipsometry.

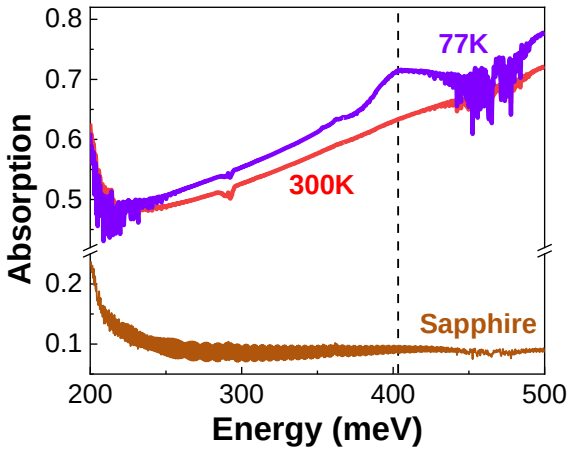

Figure S4: FTIR absorption of the 5QL SL sample. Both room temperature (300K, in red) and 77K measurements (in purple) were made. A trace of the sapphire substrate at 300K (brown) is also shown. A clear absorption transition is seen at ~400 meV in the sample when measured at 77K.

D. Theoretical Modeling

The low energy properties of both Bi_2Se_3 and Sb_2Te_3 are well described by the effective k.p Hamiltonian introduced by Zhang et al. [15] In a basis of orbital and spin degrees of freedom (represented by Pauli matrices τ^i and σ^i, respectively), the corresponding bulk tight-binding Hamiltonian can be written, in terms of the wavevector $\boldsymbol{p}$, as

$$\mathcal{H}_{tb}(\boldsymbol{p}) = C_0 + \sum_i C_i \cos(p_i a_i) + \tau^1 \sum_i v_i \sin(p_i a_i)\sigma^i + \tau^3 (M_0 + \sum_i M_i \cos(p_i a_i))$$

where $a_1 = a_2$ is the lattice spacing in the x and y directions within a given layer (4.14 Å for Bi_2Se_3, and 4.25 Å for Sb_2Te_3) and a_3 is the distance between QLs in the direction perpendicular to the alternating layers (9.55 Å for Bi_2Se_3, and 10.12 Å for Sb_2Te_3). The rest of the model fitting parameters for the two materials considered are shown in Table 1. [16]

	$v_\parallel \equiv v_1 = v_2$	v_3	C_0	$C_\parallel \equiv C_1 = C_2$	C_3	M_0	$M_\parallel \equiv M_1 = M_2$	M_3
Bi_2Se_3	0.606	0.481	3.056	-1.623	-0.031	7.026	-3.428	-0.340
Sb_2Te_3	0.869	0.290	-1.523	0.772	0.278	11.702	-5.683	-0.519

Table 1: Parameters (given in eV) for the two materials considered in the model.

Rewriting the Hamiltonian in the form $\mathcal{H}_{tb}(\boldsymbol{p}) = H_{os}(\boldsymbol{p}_{\parallel}) + \Gamma(\boldsymbol{p}_{\parallel})e^{-ip_3a_3} + \Gamma^{\dagger}(\boldsymbol{p}_{\parallel})e^{ip_3a_3}$,

the lattice adaptation along the z-direction within a given SL layer, for a given energy E, is constructed via the recursive relation, $\Gamma\psi_{n-1} + H_{os}\psi_n + \Gamma^{\dagger}\psi_{n+1} = E\psi_n$,connecting the wave function at the n_{th} lattice site, ψ_n, to its nearest neighbors. In between SL layers, the hopping matrices Γ are taken to be the average of those within the two layers. The eigen-energies are then obtained through numerical exact diagonalization of the resulting $4N(n_1+n_2)$ by $4N(n_1+n_2)$ lattice Hamiltonian (where N is number is the total number of supercells, and n_1 and n_2 are the thicknesses of the two layers forming a supercell).

References:

1. Levy, I.; Garcia, T. A.; Shafique, S.; Tamargo, M. C. Reduced twinning and surface roughness of Bi_2Se_3 and Bi_2Te_3 layers grown by molecular beam epitaxy on sapphire substrates, *J. Vac. Sci. Technol., B* **2018,** 36, 02D107.

2. Vandenberg, J. M.; Hamm, R. A.; Macrander, A. T.; Panish, M. B.; Temkin, H. Structural characterization of GaInAs(P)/InP quantum well structures grown by gas source molecular beam epitaxy, *Appl. Phys. Lett.* **1986,** 48, 1153.

3. Li, C-Z.; Li, J-G.; Wang, L-X.; Zhang, L.; Zhang J-M.; Yu, D.; Liao, Z-M. Two-carrier transport induced Hall anomaly and large tunable magnetoresistance in Dirac semimetal Cd_3As_2 nanoplates, *ACS Nano* **2016**, 10, 6020

4. Eschbach, M.; Mlynczak, E.; Kellner, J.; Kampmeier, J.; Lanius, M.; Neumann, E.; Weyrich, C.; Gehlmann, M.; Gospodaric, P.; Doring, S. et al., Realization of a vertical topological p-n junction in epitaxial Sb_2Te_3/Bi_2Te_3 heterostructure, *Nat. Comm.* **2015**, 6, 8816

5. Dubrovka, A.; Caha, O.; Hroncek, M.; Fris, P.; Orlita, M.; Holy, V.; Steiner, H.; Bauer, G.; Springholz, G. and Humlicek, J., Interband absorption edge in the topological insulators $Bi_2(Te_{1-x}Se_x)_3$, *Phys. Rev. B* **2017**, 96, 235202

6. Post, K. W.; Chapler, B. C.; He, L.; Kou, X.; Wang, K. L. and Basov, D. N. Thickness-dependent bulk electronic properties in Bi_2Se_3 thin films revealed by infrared spectroscopy, *Phys. Rev. B* **2013**, 88, 075121

7. Sehr, R. and Testardi, L.R. The optical properties of p-type Bi_2Te_3-Sb_2Te_3 alloys between 2-15 microns, *J. Phys. Chem. Solids* **1962**, 23, 1219

8. Kulbachinski, V.A.; Ozaki, H.; Miyahara, Y. and Funagai, K. A tunneling spectroscopy study of the temperature dependence of the forbidden band in Bi_2Te_3 and Sb_2Te_3, *J. Exp. Theor. Phys.* **2003**, 97, 1212

9. Köhler, H. and Hartmann, J. Burstein shift of the absorption edge in n-Bi_2Se_3, *Phys. Stat. Sol. (b)* **1974**, 63, 171

10. Stordeur, M.; Stolzer, M.; Sobott, H. and Riede, V. Investigation of the valence band structure of thermoelectric $(Bi_{1-x}Sb_x)_2Te_3$ single crystals, *Phys. Stat. Sol. (b)* **1988**, 150, 165

11. von Middensdorff, A.; Dietrich, K. and Landwehr, G. Shubnikov-de Haas effect in p-type Sb_2Te_3, *Solid State Commun.* **1973**, 13, 443

12. Martinez, G.; Piot, B.A.; Hakl, M.; Potemski, M.; Hor, Y.S.; Materna, A.; Strzelecka, S.G.; Hruban, A.; Caha,, O.; Novak, J. et al., Determination of the energy band gap of Bi_2Se_3, *Sci. Rep.* **2017**, 7, 6891

13. Orlita, M.; Piot, B. A.; Martinez, G.; Sampath Kumar, N. K.; Faugeras, C.; Potemski, M.; Michel, C.; Hankiewicz, E. M.; Brauner, T. et al., Magneto-Optics of massive Dirac fermions in bulk Bi_2Se_3, *Phys. Rev. Lett.* **2015**, 114, 186401

14. Wang, G. and Cagin, T., Electronic structure of the thermoelectric materials Bi_2Te_3 and Sb_2Te_3 from first-principles calculations, *Phys. Rev. B* **2007**, 76, 075201

15. Liu, C. X.; Qi, X. L.; Zhang, H.; Dai, X.; Fang, Z.; Zhang, S. C. Model Hamiltonian for topological insulators, *Phys. Rev. B* **2010,** 82, 045122.

16. Nechaev, I. A. and Krasovskii, E. E. Relativistic k . p Hamiltonians for centrosymmetric topological insulators from ab initio wave functions, *Phys. Rev. B* **2016,** 94, 201410(R).